Online Appendix to "Detecting structural differences in tail dependence of financial time series"

Carsten Bormann
Karlsruhe Institute of Technology
and
Melanie Schienle
Karlsruhe Institute of Technology

APPENDIX A: Proofs

Proof of Proposition 2.

Equation (4) guarantees convergence of the empirical tail copula $\sqrt{k_{\mathbb{Z}}}\widehat{\Lambda}_{\mathbb{Z}}(x^{(1)}, x^{(2)}), \mathbb{Z} = \mathbb{X}, \mathbb{Y}$, for $(x^{(1)}, x^{(2)}), (v^{(1)}, v^{(2)}) \in \mathbb{R}^2_+$. Define

$$\widehat{\Delta}(x^{(1)}, x^{(2)}, v^{(1)}, v^{(2)}) = \sqrt{\frac{k_{\mathbb{X}} k_{\mathbb{Y}}}{k_{\mathbb{X}} + k_{\mathbb{Y}}}} \left(\widehat{\Lambda}_{\mathbb{X}}(x^{(1)}, x^{(2)}) - \widehat{\Lambda}_{\mathbb{Y}}(v^{(1)}, v^{(2)}) \right)$$

Then

$$\begin{aligned} \widehat{\Pi}(x^{(1)}, x^{(2)}, v^{(1)}, v^{(2)}) = & \sqrt{\frac{k_{\mathbb{Y}}}{k_{\mathbb{X}} + k_{\mathbb{Y}}}} \sqrt{k_{\mathbb{X}}} \left(\widehat{\Lambda}_{\mathbb{X}}(x^{(1)}, x^{(2)}) - \Lambda_{\mathbb{X}}(x^{(1)}, x^{(2)}) \right) \\ & - \sqrt{\frac{k_{\mathbb{X}}}{k_{\mathbb{X}} + k_{\mathbb{Y}}}} \sqrt{k_{\mathbb{Y}}} \left(\widehat{\Lambda}_{\mathbb{Y}}(v^{(1)}, v^{(2)}) - \Lambda_{\mathbb{Y}}(v^{(1)}, v^{(2)}) \right) \end{aligned}$$

It directly follows from Equation (4) and $\frac{k_{\mathbb{X}}}{k_{\mathbb{X}}+k_{\mathbb{Y}}} \to \lambda$ that

$$\widehat{\Pi}(x^{(1)}, x^{(2)}, v^{(1)}, v^{(2)}) \xrightarrow{w} \sqrt{1-\lambda}\mathbb{G}_{\widehat{\Lambda},\mathbb{X}}(x^{(1)}, x^{(2)}) - \sqrt{\lambda}\mathbb{G}_{\widehat{\Lambda},\mathbb{Y}}(v^{(1)}, v^{(2)}).$$

Therefore by continuous mapping theorem, it holds that

$$\int_{\mathcal{I}_m} \widehat{\Pi}(\phi, 1-\phi, \phi, 1-\phi))^2 \, \mathrm{d}\phi \xrightarrow{w} S^m$$

for $m = 1, \dots M/2$, and also due to symmetry in the limiting process, we get

$$\int_{\mathcal{I}_m} \widehat{\Pi}(\phi, 1-\phi, 1-\phi, \phi))^2 \, \mathrm{d}\phi \xrightarrow{w} S^m$$

for $m = M/2+1, \dots M$ under both, the null and the alternative.

Though, $\widehat{\Delta}$ and $\widehat{\Pi}$ coincide if and only if the null hypothesis holds true. Thus we get under the null that

$$\hat{S}^m \xrightarrow{w} S^m$$

while otherwise

$$\hat{S}^m \to \infty$$

for all $m = 1, \dots, M$. □

Proof of Proposition 2. The statement directly follows from Theorem 3.4. in Bücher and Dette (2013). □

Proof of Proposition 4.

We show that individual tests are asymptotically undersized. Due to this, grid-specific p-values need not to be perfectly dependent.

For Test 1 with M_j subsets, denote the test statistic corresponding to the minimal p-value by S_j^*, and the denote the factor of S_j^* by $\upsilon_j := (k_{\mathbb{X},j} + k_{\mathbb{Y},j})/(k_{\mathbb{X},j} k_{\mathbb{Y},j})$, where $k_{\mathbb{X},j}, k_{\mathbb{Y},j}$ denote the *realized* effective sample sizes of $\mathbb{X}$ and $\mathbb{Y}$ in the subinterval corresponding to p_j^*. Obviously,

$$\upsilon_j \leq \upsilon := (k_{\mathbb{X}} + k_{\mathbb{Y}})/(k_{\mathbb{X}} k_{\mathbb{Y}}),$$

and υ_j decreases in both $k_{\mathbb{X},j}$ and $k_{\mathbb{Y},j}$, while $k_{\mathbb{Z},j}, k_{\mathbb{Y},j}$ both decrease in the fineness of the grid ($j \to \infty$): The finer the grid, the smaller $k_{\mathbb{Z},j}$, i.e. less observations are in each subinterval. For υ, a test against copula equality would be asymptotically exact, i.e. $\mathbb{P}(p \leq \alpha | H_0) \to \alpha$, under ($A1^S$)-($A4^S$).

Realize that – under the null – the test statistic integrates over squared differences of centralized normal variables. We may approximate the right tail of the null distribution by a centered χ^2 distribution with, say, $\varpi_j > 0$, degrees of freedom; see Beran (1975). Hence, for x large enough, test size can be approximated as $\alpha_j := \mathbb{P}(\widetilde{S}_j^* > x | H_0) \sim \chi^2(\varpi_j), j = 1, ..., J$, where $\widetilde{S}_j^*$ denotes the theoretical test statistic corresponding to the adjusted p-value $\tilde{p}_j^*$. Also, for the variance of the test statistic, it holds that $\mathbb{V}(\widetilde{S}_j) = \mathcal{O}(\upsilon_j^2)$, i.e. the variance increases as grid fineness increases ($j \downarrow$) and less observations enter the estimation ($k_{\mathbb{X},j}, k_{\mathbb{Y},j} \downarrow, \upsilon_i \uparrow$). According to the Markov inequality, with fixed critical values x_j,

$$\alpha_j := \mathbb{P}(\widetilde{S}_j^* \geq x_j | H_0) \leq \frac{\mathbb{E}(\widetilde{S}_j^*)}{x_j} = \frac{\mathbb{V}(\widetilde{S}_j^*)/2}{x_j}) = \mathcal{O}(\mathbb{V}(\widetilde{S}_j^*)),$$

i.e. under the null, realized test sizes α_j decrease with rate υ_j^2. Furthermore, grid-specific p-values are continuous and uniformly distributed. Now, Sklar's

Theorem implies their dependence under the null can be characterized by a copula, C_α, say, i.e. $C_\alpha(\boldsymbol{u}) = \mathbb{P}(\tilde{p}_1^* \leq u^{(1)}, ..., \tilde{p}_J^* \leq u^{(J)}|H_0)$. Under the null, the FWER in terms of the copula C_α, is given by

$$\mathbb{P}(\cup_{j=1}^J \tilde{p}_j^* \leq \alpha|H_0) = 1 - C_\alpha(1-\alpha_1, ..., 1-\alpha_J), . \tag{1}$$

For illustration, let nearly any observations at all fall in relevant subintervals, i.e. $\forall j : \upsilon_j \approx 0$,

$$1 - C_\alpha(1-\alpha_1(\upsilon_1), ..., 1-\alpha_J(\upsilon_J)) \downarrow 1 - C_\alpha(1, ..., 1) = 0,$$

and Test 2 naturally obeys the α-limit in this unrealistic case. In all other cases, as $J \to \infty$, for FWER control $\mathbb{P}(\cup_{j=1}^J p_j^* \leq \alpha|H_0) \leq \alpha$, it must hold that

$$1 - C_\alpha(1-\alpha_1(\upsilon_1), ..., 1-\alpha_J(\upsilon_J)) \nearrow \alpha_\star(\upsilon_\star),$$

where $\alpha_\star := \max(\alpha_1(\upsilon_1), ..., \alpha_J(\upsilon_J)) \to 0$. This means, for FWER control, the copula C_α must approach its upper bound – $(\alpha_1, ..., \alpha_J)$ must be nearly perfectly dependent – but the upper bound does not need to be exactly obtained due to $\alpha_j \to 0, j = 1, ..., J$. □

APPENDIX B: Details on Specifications and Additional Simulation Results

Details on Specifications of the Simulations

DGP1 and DGP2 are based on the tail factor model. Bivariate return vectors $\mathbb{Z} = (Z^{(1)}, Z^{(2)}), \mathbb{Z} = \mathbb{X}, \mathbb{Y}$, follow a bivariate factor model with r factors $V^{(j)}, j = 1, ..., r$, and loadings $a_{ij}, i = 1, 2, j = 1, ..., r$, when

$$Z^{(i)} = \sum_{j=1}^{r} a_{ij} V^{(j)} + \varepsilon^{(i)}, i = 1, 2, \tag{2}$$

where factors are i.i.d. Fréchet with $\nu = 1$, independent of the error term $\varepsilon^{(i)}$ which feature thinner tails than $V^{(j)}$; we set $\varepsilon^{(i)}$ as Fréchet with $\nu_\varepsilon = 2$. In this way, the matrix of factor loadings $A = (a_{ij})$ directly determines the tail copula of $\mathbb{Z}$. In particular, the (upper) tail copula of $\mathbb{Z}$ is equivalent to the tail copula of the max factor model $\bar{Z}^{(i)} = \max_{j=1,...,r}(a_{ij} V^{(j)})$, which is

$$\Lambda^U(x^{(1)}, x^{(2)}) = x^{(1)} + x^{(2)} - \sum_{j=1}^{r} \max\left(\frac{a_{1j}}{\sum_{j=1}^r a_{1j}} x^{(1)}, \frac{a_{2j}}{\sum_{j=1}^r a_{2j}} x^{(2)} \right),$$

see **?** for further details. DGP1 consists of $\mathbb{X}, \mathbb{Y}$ both resulting from a factor model as in Equation (2), but with loading matrix $A_1 = \left[\begin{smallmatrix} 2 & 1 & 0 \\ 0 & 1 & 2 \end{smallmatrix}\right]$. Here, the first factor only influences $X^{(1)}$ $(Y^{(1)})$, the second factor influences both $X^{(1)}$ $(Y^{(1)})$ and $X^{(2)}$ $(Y^{(2)})$, and the third factor only influences $X^{(2)}$ $(Y^{(2)})$. That is, A_1 amounts to intra-tail symmetry and to tail equality between $\mathbb{X}$ and $\mathbb{Y}$, and thus the null is true. See Figure 3, first from the left, for $\Lambda(x^{(1)}, 1-x^{(1)}), x^{(1)} \in [0,1]$. For DGP2, both $\mathbb{X}$ and $\mathbb{Y}$ stem from a factor model as in Equation (2) with $A_2 = \left[\begin{smallmatrix} 1 & 0 \\ 1 & 2 \end{smallmatrix}\right]$, where the second factor only influences $X^{(2)}$ $(Y^{(2)})$, causing the tail copula to become intra-tail asymmetric, $\Lambda(x^{(1)}, x^{(2)}) \neq \Lambda(x^{(2)}, x^{(1)})$, and consequently tail copulas of $\mathbb{X}$ and $\mathbb{Y}$ coincide only when $x^{(1)} = x^{(2)}$, see Figure (3), second from the left. DGP2 thus represents the class of intra-tail asymmetric copulas which violate the null according to Proposition (1).

For the GARCH-type time series specification we use the following algorithm: In a first step, we simulate observations $\eta_{t,\mathbb{Z}}$ according to DGPs 1 to 4. Consequently, we transform simulated errors to pseudo-observations by means of the marginal empirical cumulative distribution, $\widehat{F}_{\eta,\mathbb{Z},i}(\eta_{t,\mathbb{Z}}^{(i)}), i = 1, 2$. Finally, we apply the quantile function of the t-distribution function with 10 degrees of freedom to the pseudo-observations. Thus, the final errors are linked by the copulas of DGPs 1 to 4 with fat-tailed t-marginals. Those are used to generate the GARCH series for $\mathbb{X}$ and $\mathbb{Y}$, and standardized residuals obtained from estimation by quasi maximum likelihood. Note, monotone transformations, such as the quantile transformation, do not alter the tail dependence structure, and should not alter test results. However, t-transformed error distributions are a more realistic approximation of asset returns.

Additional Simulation Results

The simulation results in Figure 1 Appx below confirm that the key Condition 7 for the consistency of the aggregated Test (2) in Proposition 4 appears to be satisfied in standard settings. We find Test 2 consistently obeys the α-limit due to individual undersizedness of Test 1 and nearly perfect dependence between grid-minimal p-values Figure 1 Appx shows p-values of one specific setting, which illustrates that both these points hold; results of other settings are in line, but not reported. We see that individual test sizes are consistently below α, and decrease in the number of marginal hypotheses. Furthermore, correlation between minimal p-values of different grids is close to one, indicating nearly perfect (linear) dependence. Hence, we find Test 2 is appropriate.

Table (1 Appx) provides additional simulation results for the smaller sample size $n = 750$. The same set-up and specifications as for Table 1 in the paper are used and empirical test rejections are reported.

Additionally for time series, we investigate the performance of the tapered multiplier bootstrap for tail copulas in comparison to the GARCH filter approach. For simulated GARCH time series with error terms linked by the Clayton copula with $\theta = 0.5$, and the Factor copula with loading matrix A_1, we estimate

Figure 1 Appx: Exemplary p-values from the simulation study for Test 1 with $j = 1, ..., 13$ (GARCH marginals equipped with a Factor model, $k = 0.1n, n = 1500$, tapered bootstrap). In this case, test size is estimated with 500 repetitions. Left: Scatterplots of p-values for all grid pairs. Middle: J, the fineness of the grids, is plotted against estimated test sizes according to Test 1. Right: Histogram of estimated correlations between all pairs of grid-minimal p-values.

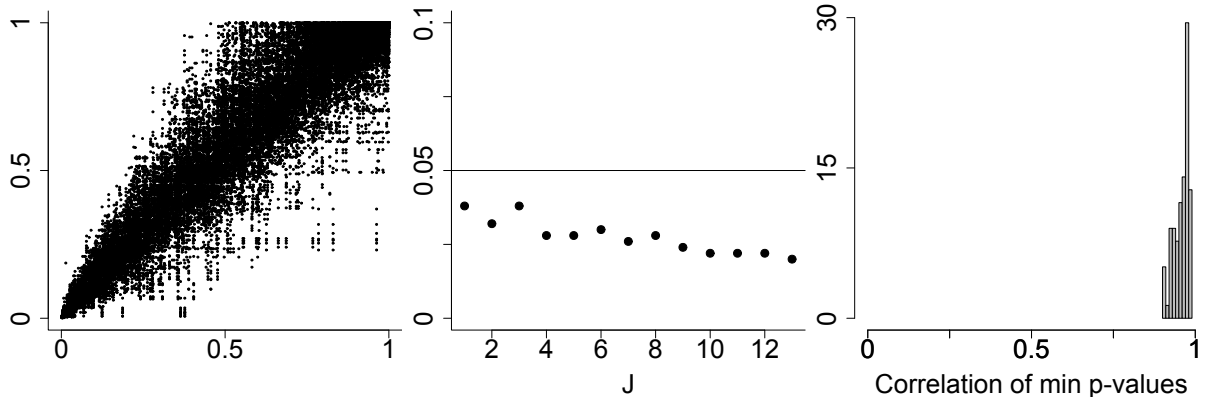

the tail copula with the underlying i.i.d. data, (correctly) GARCH filtered data, and we apply the tapered bootstrap to unfiltered data. Table (2 Appx) shows bias and variance for all three approaches. While the tapered bootstrap exhibits a higher variance, its bias is consistently smaller. Thus, we find the tapered bootstrap approach successfully approximates the tail copula in the presence of GARCH effects.

APPENDIX C: Tail Asymmetries in the US Stock Market with GARCH Filtering

The U.S. stock market application in Section 5 of the paper only reports test results for the tapered multiplier bootstrap. For completeness, we here provide results for an adaptive GARCH filter in combination with the standard multiplier bootstrap. For each stock sector, and in each period, we fit ARMA(p_1, q_1)-APARCH(p_2, q_2)-models, $p_1, q_1 = 0, 1, 2, p_2, q_2 = 0, 1$ with Skew Student-t error term distributions. We choose an optimal model according to the AIC. Standardized residuals are used for the test. This approach captures potential asymmetric GARCH-effects, Ding et al. (1993). Figure (2 Appx) shows the test results.

Trajectories strongly resemble those of the tapered multiplier approach (Figure (5)), except for the financial crisis 2007-09 when results diverge. GARCH-filtered data exhibits more tail inequalities. This also adds to the unique, anomalous nature of this crisis as eliminating GARCH-effects induces additional heterogeneity between the tails. Thus, results confirm that the use of the direct

Table 1 Appx: Empirical rejection probabilities as in Table (1), but with a sample size of $n = 750$.

k/n	DGP1					DGP2					DGP3					DGP4				
	TDC	BD13	BS16			TDC	BD13	BS16			TDC	BD13	BS16			TDC	BD13	BS16		
			18	6	TA2			18	6	TA2			18	6	TA2			18	6	TA2
iid																				
5%	4.6	4.8	3.6	3.8	5.6	2.6	4.4	97.8	100	99.8	3.4	4.0	3.6	3.2	6.2	43.2	57.8	44.6	52.2	60.8
10%	3.2	2.8	2.6	2.2	5.0	5.4	5.8	100	100	100	3.4	3.6	2.8	3.2	6.0	65.2	79.6	69.6	75.8	82.4
15%	4.0	4.2	3.2	2.8	7.2	4.2	5.6	100	100	100	4.0	5.8	2.8	3.4	8.0	76.4	86.2	81.0	83.6	88.6
tap.																				
5%	5.0	6.2	4.2	4.6	6.8	4.4	3.8	98.0	78.6	99.8	11.6	15.2	13.8	13.8	20.4	26.6	39.4	33.4	37.0	44.8
10%	4.4	5.4	3.0	4.4	7.2	4.8	6.2	100	100	100	8.0	12.6	12.4	12.2	19.4	48.2	61.4	55.8	57.8	66.2
15%	2.4	4.2	3.2	3.6	5.6	6.2	6.4	100	100	100	8.2	9.8	7.6	8.0	13.8	62.0	75.4	69.6	73.2	79.6

Table 2 Appx: Integrated squared bias and variance for i.i.d. and GARCH filtered data, and the tapered bootstrap approach. Simulations have been repeated 500 times with $n = 1500$ and $k \sim U[0.05n, 0.15n]$. For the Clayton copula, we choose $\theta = 0.5$, and the factor model was parametrized by Results are scaled by loading matrix A_1. 10^{-2}.

	i.i.d.	filter	tapered		i.i.d.	filter	tapered
Clayton				Factor			
bias^2	1.374	1.297	0.710		0.050	0.048	0.002
variance	0.039	0.040	0.083		0.010	0.010	0.049

tapered multiplier bootstrap specification in the paper works and that obtained results can be safely interpreted.

APPENDIX D: Tests for Tail Asymmetries in the US Stock Market

The difference in found asymmetries between our test and BD13 (see Figure 5 of the paper) suggests some degree of intra-tail asymmetry among all pairs. The simulation study demonstrated that the power of the two tests differs mainly in intra-tail asymmetric cases, see Table 1 in the paper, but also Table 1 Appx.

Here, we apply two formal tests against intra-tail symmetry (Kojadinovic and Yan (2012); Bormann (2017)) in order to fully quantify the importance of intra-tail asymmetries for tail asymmetries. Both test check the (tail) copula

Figure 2 Appx: Dynamics of the percentage of detected tail asymmetries among all pairs. Data has been filtered using an adaptive GARCH filter, using a rolling window of size $n = 1500$, and a step size of 250 trading days for the TDC test (dashed), BD13 test (dotted) and our test (solid), respectively.

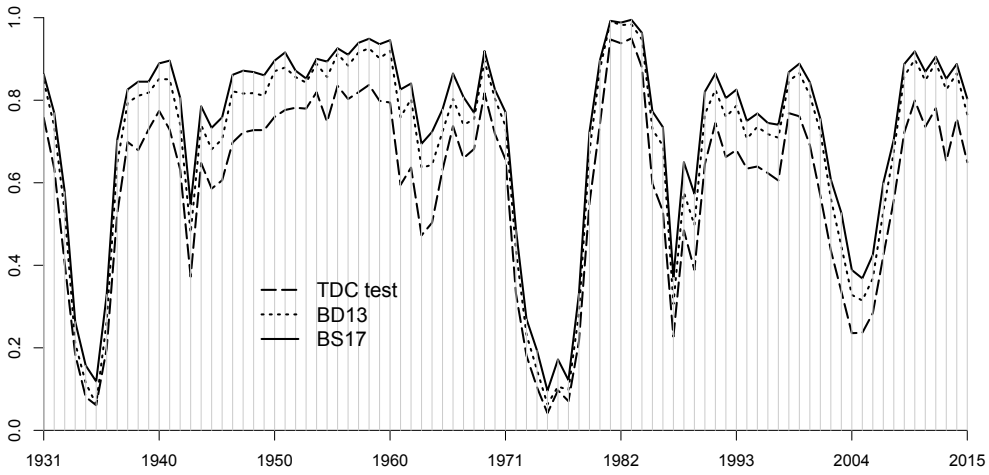

against non-exchangeability with Cramér-von Mises tests, while the latter tests explicitly accounts for serial dependence, and is thus more appropriate here. We use a significance level of $\alpha = 0.05$. For periods with the smallest and the largest discrepancy in the number of test rejections between our test and the BD13 and the TDC test, respectively, we test for intra-tail asymmetries. Table 3 Appx contains the test results. Intra-tail asymmetry of a sector implies one sector's extremes are more likely to trigger extreme events of the other sector. This demands special care in hedging as anticipation of (conditional) extremes is uneven. For small (large) discrepancies, we expect no (a) significant portion of test rejections. When our test does not find substantially more tail asymmetries than BD13 during 1975–81 (TDC during 1977-83), we detect only 4.1% (3.5%) intra-tail asymmetric pairs. On the other hand, this share rises to 12.5% (9.13%) when our test is more powerful with respect to detecting tail asymmetry (BD13 during 1938–1943, TDC during 1945–51). Although the share of found intra-tail asymmetries is relatively small, this supports the conjecture that intra-tail asymmetry explains the differences in test results.

APPENDIX E: Tail Inequalities of Foreign Exchange Rates

To supplement the empirical study on tail asymmetries on stock markets in Section 5, we now analyze tail equality in pairs of six main foreign exchange ra-

Table 3 Appx: ITA test results. We test against ITA in periods when results of our test and competing tests are most (least) similar, i.e. when the shares of test rejections is the largest (the closest). See also Figure 5. In such periods, we report the share of bivariate tails that the test identifies as intra-asymmetric.

	BD13		TDC	
test results	period	ITA	period	ITA
similar	1975-81	4.1%	1977-83	3.5%
maximally different	1938-43	12.5%	1945-51	9.13%

tes, namely Euro (EUR), British Pound (GBP), Canadian Dollar (CAD), Japanese Yen (JPY), New Zealand Dollar (NZD) and Swiss Franc (CHF), all nominated in USD. Time series data are standard exchange rates from Bloomberg. The sample consists of returns of daily closing prices covering the period 01/05/2001 to 02/01/2016. As foreign exchange rates are the most frequently traded financial security with an average daily trading volume of more than five trillion in April 2013 (Rime and Schrimpf (2013)), investors and regulators have a natural interest in a comparison of extreme co-movements of foreign exchange rates. We again apply a rolling window analysis, now with a window size of $n = 1000$ and step size of 50 days to draw a finer picture of the tail (in)equality dynamics. For any pair comparison trading days with missing data or zero returns are discarded. The effective sample size is fixed $k = 0.2n$ which is backed by the results of the simulation study. We conduct the following tail pair comparisons

$$H_0^{(L-L)} : \Lambda_{\mathbb{X}}^L = \Lambda_{\mathbb{Y}}^L, \quad H_0^{(L-U)} : \Lambda_{\mathbb{X}}^L = \Lambda_{\mathbb{Y}}^U, \quad H_0^{(U-U)} : \Lambda_{\mathbb{X}}^U = \Lambda_{\mathbb{Y}}^U,$$

for all 15 bivariate pairs, amounting to $4 \cdot \binom{6}{2} = 420$ tests in each period. Note, this also implies the null hypotheses $H_0^{(U-L)} : \Lambda_{\mathbb{X}}^U = \Lambda_{\mathbb{Y}}^L$. Figure (4 Appx) shows the share of tail inequalities among all possible comparisons. The fraction of rejected tail equalities, ranging from 45% to 75%, suggests bivariate tail dependence of foreign exchange rates systematically differ. We observe a steady increase of tail inequalities from 2006 to 2008 which coincides with a major depreciation of the USD with respect to the EUR. This evolution is reversed when the USD appreciates during the European Sovereign Crisis (2013 onwards). Thus, in the last decade, a strong (weak) USD (EUR) came along with more (less) tail equality within the foreign exchange rates market.

Figure (5 Appx) displays a dynamic ranking for all 15 pairs based on the TDC and the summary statistic $\int_0^1 \Lambda(\phi, 1-\phi)\mathrm{d}\phi$ which was introduced in the last subsection. A careful inspection of all four plots shows there is only little difference between the TDC-based and the tail copula-based ranking. Tail dependence of

appreciations and depreciations of EUR and CHF with respect to the USD tends to be the strongest throughout the sample. While the pair GBP-EUR exhibits strong tail dependence for joint upper tails (depreciations), the lower tails show a strong tail link only in the last five years (as well as until 2007). Also, JPY-CAD (upper tail) and CAD-NZD (both tails) feature comparably strongly connected tails. The pairs JPY-NZD, JPY-CAD and GBP-JPY feature the weakest tail dependence in both tails.

The pair EUR-CHF dominates tail comparisons throughout, which is probably due to the fixed exchange rate regime until 01/2015 with a EUR:CHF minimum rate of $1{:}1.20$. Also, the tight economic linkage between both parties may attribute to the relatively strong tail dependence. On 01/15/2015, the Swiss Central Bank unpegged its currency from the Euro. This policy change caused the CHF to appreciate by 20% with regards to the EUR within a single day.

We now test whether the break of the CHF-EUR currency peg had a significant impact on the tail dependence between both currencies. This would be the case if the TC had changed after 15/01/2015. Unfortunately, the sample contains only 273 observations after the policy change and we thus compare TCs for overlapping time periods, that is 01/01/2006 - 14/01/2015 (Λ^{T1}) and 01/01/2006 - 16/01/2016 ($\Lambda^{T1,T2}$). The null is

$$H_0 : \Lambda^{W,T1}_{CHF-EUR} = \Lambda^{W,T1+T2}_{CHF-EUR}, W = U, L \tag{3}$$

However, the tapered block multiplier bootstrap has to be adjusted to account for the dependence of both samples. For the tail copula of the entire period ($T_1 + T_2$), we use the multiplier vector $\xi^{T1+T2} = (\xi_1, ..., \xi_{T1}, \xi_{T1+1}, ..., \xi_{T1+T2})$; for the tail copula of the first subperiod, we only use the first T_1 entries of ξ^{T1+T2}. We execute the test for 15 different values of the effective sample size, namely $k_{Ti} = 0.02n_{Ti}, 0.04n_{Ti}, ..., 0.3n_{Ti}, i = 1, 2$, where n_{Ti} denotes the sample size of the first subperiod (T_1) and the entire period (T_2), respectively. Table (4 Appx) contains p-values of Test (2). To this date, there is no evidence for a structural change in neither the lower nor the right tail.

Table 4 Appx: P-values corresponding to the null hypothesis of constant tail dependence between EUR and CHF (see Equation (3)) for varying effective sample sizes.

k/n tails	0.02	0.04	0.06	0.08	0.10	0.12	0.14	0.16	0.18	0.20	0.22	0.24	0.26	0.28	0.30
L-L	4.4	10.6	37.2	30.8	17.9	19.9	22.4	35.6	52.0	61.5	46.2	33.6	46.0	56.1	63.7
U-U	99.2	7.4	98.0	87.2	99.9	87.8	44.7	80.2	98.6	99.6	95.7	96.1	99.8	99.6	96.6

Figure 3 Appx: Foreign exchange rates nominated in US Dollars during 01/2001 - 02/2016.

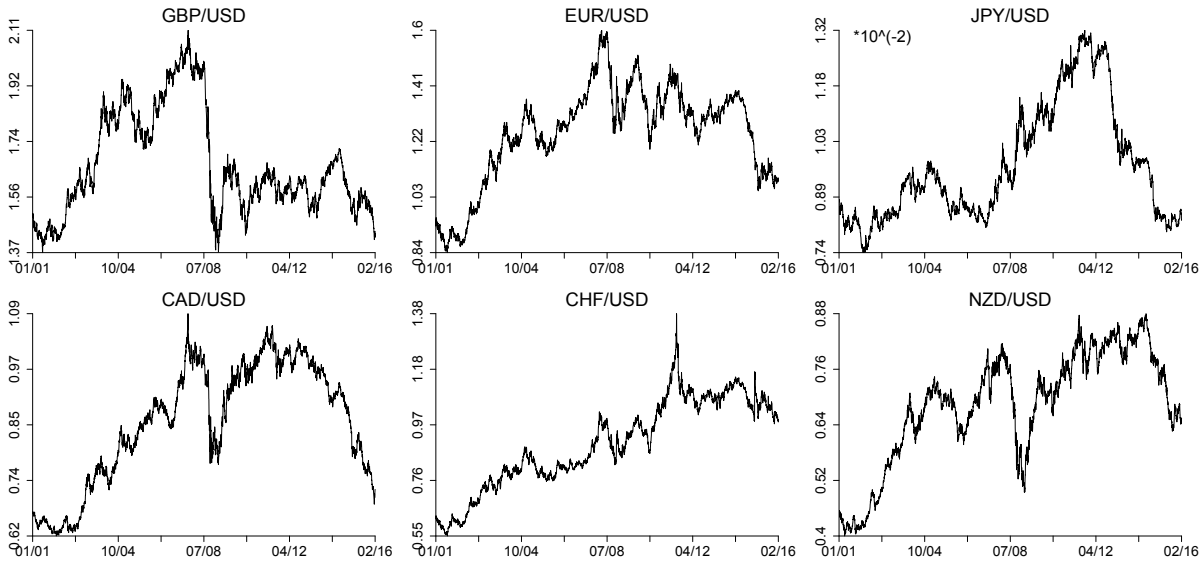

Figure 4 Appx: Dynamics of the percentage of detected tail inequalities among all pairs, comparing the following tails: Upper-upper, upper-lower, lower-lower. The window size is $n = 1000$ with a step size of 50 trading days, and rejections based on the TDC test (BD13 test, our test) correspond to the dashed (dotted, solid) line.

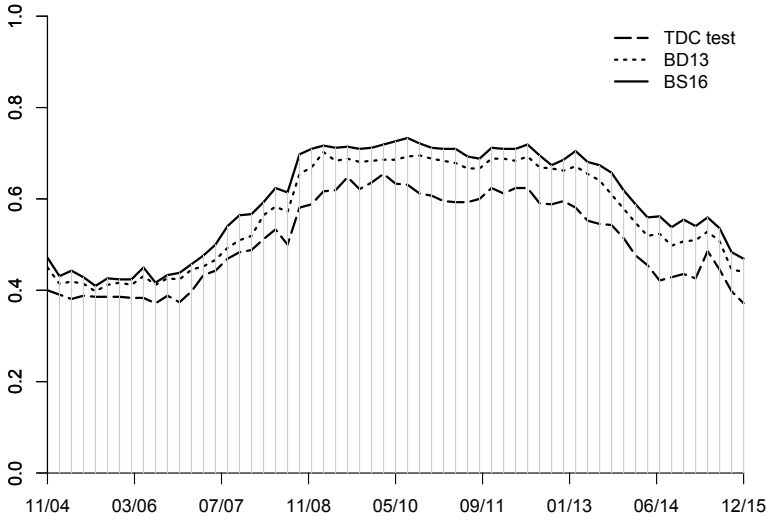

Figure 5 Appx: Tail dependence ranking of all 15 pairs for the lower (left column) and upper (right column) tails according to the summary statistic $\int_0^1 \Lambda(\phi, 1-\phi)\mathrm{d}\phi$ (top row) and the TDC (bottom row), respectively. The size of each dot reflects the rank. For each period, the diamond shaped dots mark the strongest pair.

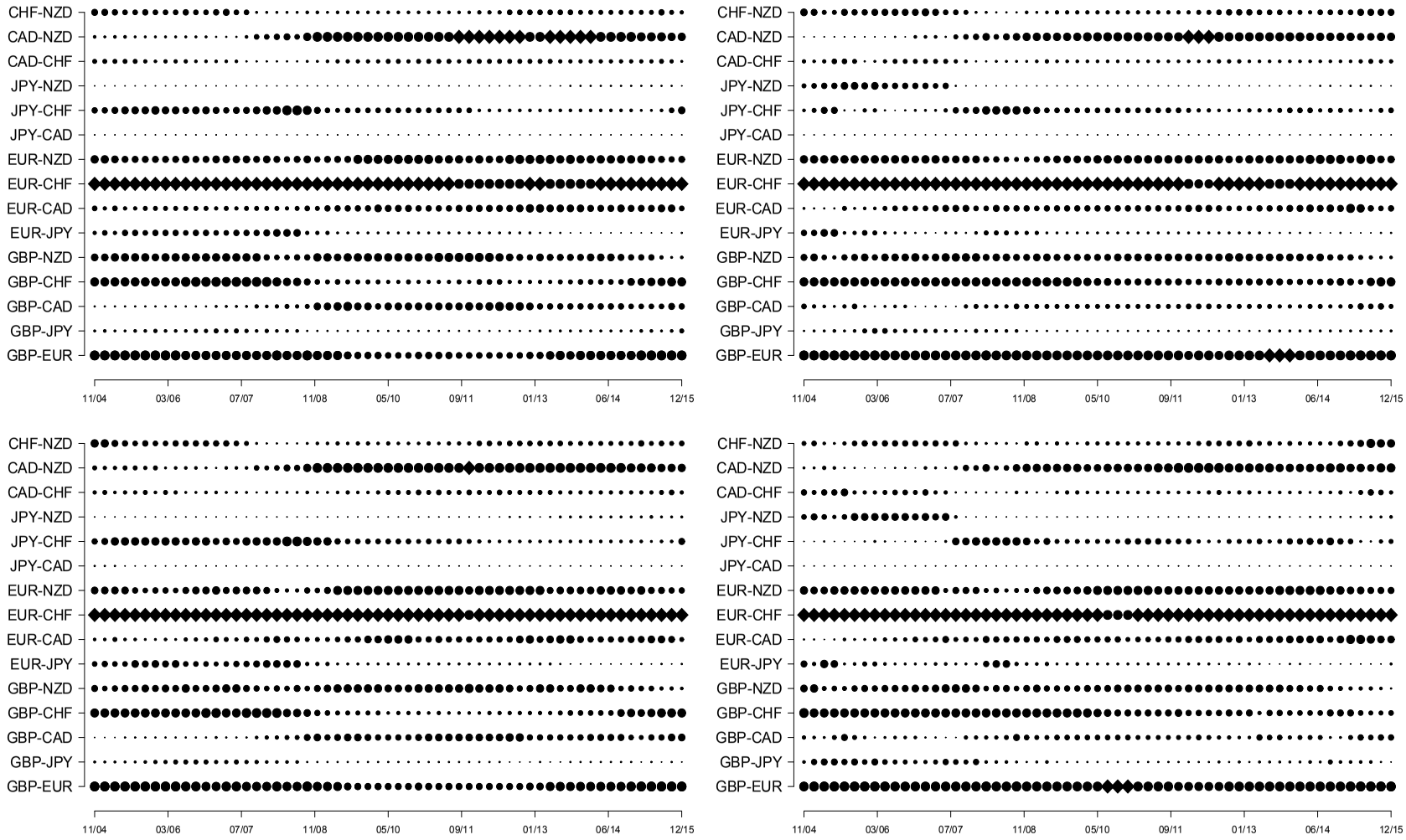

References

Beran, R. (1975), “Tail probabilities of noncentral quadratic forms,” *Annals of Statistics*, 3(4), 969-974.

Bormann, C. (2017), “Testing against intra-tail asymmetries in financial time series,” KIT Working Paper.

Bücher, A., and H. Dette (2013), “Multiplier bootstrap of tail copulas with applications,” *Bernoulli*, 19(5A), 1655-1687.

Ding, Z., C. W. Granger, and R. F. Engle (1993), “Forecasting financial assets volatility using integrated GARCH-type models: International evidence,” *Journal of Empirical Finance* , 1, 83-106.

Kojadinovic, I. and J. Yan (2012), "A non-parametric test of exchangeability for extreme-value and left-tail decreasing bivariate copulas," *Scandinavian Journal of Statistics*, 39, 480-496.

Rime, D. and A. Schrimpf (2013), “The anatomy of the global FX market through the lens of the 2013 Triennial Survey,” *BIS Quarterly Review*, December, 27-44.